Treating interactions between polarons and oxygen vacancies in perovskite oxides

Dylan Windsor [*] and Haixuan Xu [†]
University of Tennessee–Knoxville, Knoxville, Tennessee 37996, USA

(Received 8 April 2024; accepted 16 August 2024; published 13 September 2024)

Interactions between polarons and oxygen vacancies in oxides, which cause them to modify one another's physical properties, are highly important for applications such as photovoltaics and ferroelectrics. While the difficulty in modeling polarons using density functional theory (DFT) calculations has been alleviated by the recent development of various techniques, including, e.g., the Hubbard-U parameter and finite-size corrections, the underlying physics of polaron interactions with defects remains unknown. Here, we demonstrate that the polaron-vacancy complexes in $PbTiO_3$ have a preferred orbital configuration, different from the orbital configuration of the bulk polaron, by exploring multiple nearby local minima using DFT + U. To address the issue of polaron property dependence on the Hubbard-U value, we determine the U value via enforcement of piecewise linearity, and we employ finite-size corrections. Three local minima with different electronic configurations are found by varying the initial conditions: (i) a polaron trapped in a Ti-3d_{eg} orbital on the first-nearest-neighbor Ti-ion of the oxygen vacancy (*eg* complex), (ii) a polaron trapped in a Ti-3d_{t2g} orbital at the same position ($t2g$ complex), and (iii) electrons delocalized across several nearby sites and both spin channels, resulting in a semilocalized state. We find that the *eg* complex is the most energetically favorable state, revealing a change in the orbital of the polaron when trapped by an oxygen vacancy, since the bulk polaron is found to be in a $t2g$ orbital. Furthermore, we demonstrate that great care must be taken to find the correct physical picture with DFT + U, since a small change in the initial conditions results in finding different local minima.

DOI: 10.1103/PhysRevMaterials.8.094406

I. INTRODUCTION

Polarons are defined as the quasiparticle representation of a charge carrier trapped by lattice distortions, and they are known to govern effects such as charge transfer [1], multiferroism [1], and surface reactivity [2]. For practical applications, polarons can be trapped by microstructural features and defects in materials, such as oxygen vacancies, which are well-known defects ubiquitous in transition-metal oxides. While it has been demonstrated that these two types of defects coexist and interact both in allotropes of TiO_2 [2] and CeO_2 [3] near their respective surfaces, and in the bulk of CeO_2 [4] and $SrTiO_3$ [5], the role of polaron-vacancy interactions (PVIs) is not fully understood [Fig. 1(a)]. Given the wide range of phenomena affected by these two defects, it is of vital importance to fundamentally understand PVIs, which are critical for electron transport, carrier recombination, and other functional properties sought after in photovoltaic and memory technologies [4,6].

The recent decades have borne important advances in DFT treatments of both polarons and point defects [7] by moving beyond standard DFT. While standard DFT has proved an unprecedentedly useful tool for predicting point defect properties [7], it suffers from a well-known self-interaction error and misrepresented Coulomb repulsion [1,7], which precludes its ability to accurately predict properties of systems with highly correlated electrons and localized charge [1,7]. There are several options available to overcome the self-interaction error and correct the delocalized picture it results in, including DFT + U [8], the so-called self-interaction correction (SIC) scheme [9,10], and hybrid functionals [11], in order of ascending computational cost. Both DFT + U and hybrid functionals are known to provide accurate predictions of polaron and defect properties [12,13] and provide excellent explanatory power for experimental results. While hybrid functionals are the more accurate option and are sometimes used to benchmark DFT + U calculations, their computational cost is prohibitive when larger systems are required to obtain more accurate physical pictures, as has been argued in studies of polarons [12,14]. Additionally, the study of defects increases the computational cost of calculations, since they require larger supercells to accurately determine their properties, further multiplying the already large computational cost of hybrid functional calculations. On the other hand, DFT + U is considerably more computationally efficient and has been shown to match even hybrid functional accuracy [1,7,15,16], given a well-chosen Hubbard-U parameter. DFT + U, therefore, is of indispensable utility for increasing our understanding of the mechanisms by which PVIs may be controlled.

This choice of the Hubbard-U parameter has important implications for the system, since the value of many properties has been shown to depend on the U value chosen [13]. Indeed, Setvin *et al.* [13] showed a change in the polaron trapping energy of up to ∼0.2 eV in TiO_2 for every 1 eV difference in the U parameter chosen. The Hubbard-U is often chosen by matching to empirical data, such as the band gap [1], more

[*]Contact author: dwindso1@vols.utk.edu
[†]Contact author: xhx@utk.edu

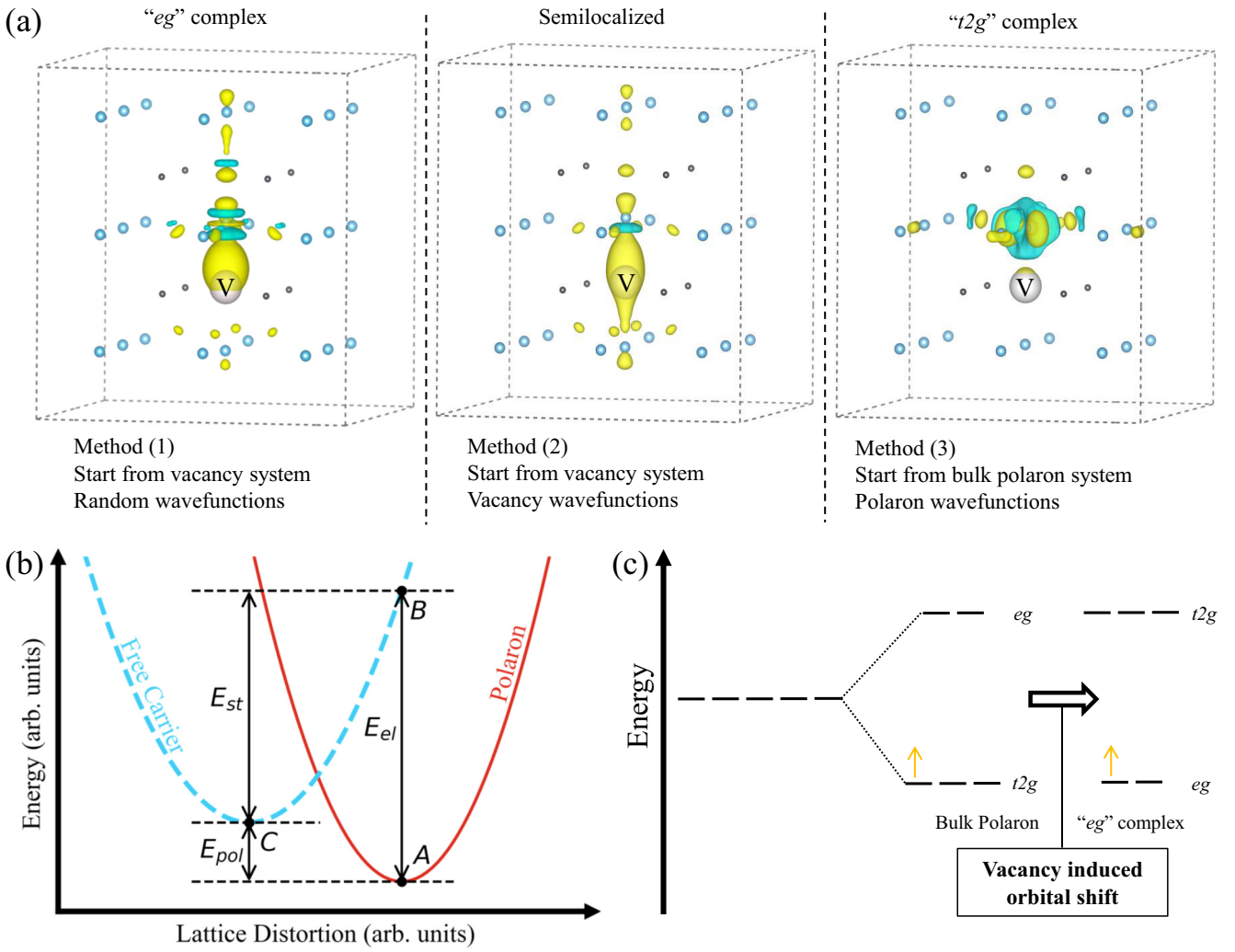

FIG. 1. (a) Varying the initial conditions of the calculation of a polaron-vacancy complex (PVC) results in three distinct configurations. For example, Method (1) involves starting from the vacancy system with random wavefunctions to obtain the "*eg*" complex. Note the oxygen atoms have been removed to more easily view the charge density structure of the polarons. (b) The representation of a polaron in DFT, where the polaron and free carrier systems are compared as the competition between two energies: the structural distortion cost (E_{st}) and the electronic energy (E_{el}), where the difference is the polaron trapping energy. These energies are calculated by comparing the energy of the system containing a polaron (A) with the delocalized system in the polaron configuration (B) and the system with a free carrier (C). (c) The PVI appears to affect the orbital degree of freedom by lowering the energy of an electron occupying a $t2g$ orbital in the "$t2g$" complex case but decreases the energy of an electron occupying an eg orbital in the "*eg*" complex, a primary difference between the PVCs.

accurate functionals [12], or by self-consistent calculation [17]. However, a recently published study by Falletta *et al.* [16] proposed a method for calculating the Hubbard-U by constraining its value via Janak's theorem [18]. The resulting U value (U_k in Falletta's notation) is thereby constrained by the enforcement of piecewise linearity (PWL), which is shown to lead to polaron trapping energies in close agreement with the hybrid functionals. For example, the defect formation energies and ionic structures of polarons calculated by hybrid and DFT + U have been shown to agree closely in $BiVO_4$, MgO, MgO (Li substitution), and α-SiO_2 (Al substitution) [16].

To calculate pertinent quantities to the energetics of polarons within DFT + U, the differences between several systems are considered [Fig. 1(b)]. The energy differences among these systems give the polaron trapping energy, $E_{\rm pol}$, as the competition between the structural energy, $E_{\rm st}$, required to distort the lattice into the polaron configuration and the energy of the transition between the charge being localized and delocalized, $E_{\rm el}$, at the ionic site of interest:

$$E_{\rm pol} = E_{\rm el} - E_{\rm st}. \tag{1}$$

This theoretical picture is connected to experiments via the $E_{\rm el}$ term, which may be compared to experiments to validate the DFT results, since in the timescale of the experiment the lattice does not have time to relax [1]. This is demonstrated by Setvin *et al.* [13], where DFT + U is used to successfully calculate $E_{\rm el}$ and compares well with experimental results by low-temperature scanning-tunneling microscopy/spectroscopy (STM/STS) measurements. This work showed experimental validation for previous work done by Janotti *et al.* [19] using hybrid functionals to calculate

the polaron trapping energies in rutile TiO_2, where charged defects, including vacancies, were shown to impact the formation and binding energies of polarons in TiO_2, leading to the conclusion that charged defects and polarons should be treated as defect complexes. In another work, Janotti *et al.* [5,19] further strengthen the importance of treating charged defects, particularly oxygen vacancies, as a complex with polarons present in $SrTiO_3$. We therefore investigate the energetics and structure of polaron-vacancy complexes (PVCs), using $PbTiO_3$ as a model system since there are few studies involving polarons in this material [12].

In this work, we study the interactions between charged oxygen vacancies and polarons in $PbTiO_3$ (PTO), a prototypical ferroelectric material known to host both polarons [12,20] and oxygen vacancies, and we explore various recipes for treating PVCs therein. As a highly important industrial material, PTO forms one of the backbones of the ferroelectric and piezoelectric industry alongside, and as a component of, $Pb(Ti_xZr_{1-x})O_3$. In PTO, properties ranging from optical transitions [20] to multiferroism [21,22] are shown to depend on both vacancies and polarons. For instance, Zhang *et al.* [23] demonstrated via DFT + U that oxygen vacancy formation energy depends on the distortion of the lattice in a $SrTiO_3/PbTiO_3$ heterostructure. Additionally, the recombination of conduction holes with electron polarons in PTO has been demonstrated by both hybrid and DFT + U calculations [12], predicting a luminescence peak at 2.49 eV, in close agreement with the 2.38 eV reported by experiment [20]. Therefore, as charge trapping in the lattice affects, by definition, the ferroelectric and piezoelectric properties, we study the polaron-vacancy interactions in the PTO lattice by exploring several local minima, which are reached by initializing random wave functions in a vacancy system, adding a polaron to a vacancy system, and adding a vacancy to a polaron system. We carefully examine each case in succession, using multiple levels of analysis: comparing spin and charge densities, local ionic structures, electronic structures, and defect transfer levels. We then compare these complexes to the isolated (bulk) polaron and bulk vacancy calculations to infer the interaction phenomena.

II. METHODOLOGY

We perform all DFT simulations using the Vienna *ab initio* simulations package (VASP) [24,25]. The generalized gradient approximation (GGA) functional used for all complex, polaron, and vacancy system calculations is the PBEsol [26] functional. Based on the work of Ghorbani *et al.* [12] and Zhang *et al.* [27], a $3 \times 3 \times 3$ supercell is used for all systems alongside a $4 \times 4 \times 4$ Γ-centered *k-point* grid, since it maintains accuracy and computational efficiency for both polaron and vacancy calculations. The energy cutoff is 550 eV. Planar-augmented-wave (PAW) basis [28] composed pseudopotentials are used for each species with the following valence electron configurations: Ti *3p3d4s* ($10\,e^-$), O *2s2p* ($6\,e^-$), and Pb *5d6s6p* ($14\,e^-$). Each relaxation and self-consistent field calculation was converged to Hellmann-Feynman forces of $<0.01\,eV/Å$ and to a total energy difference of $<10^{-8}\,eV$. Furthermore, finite-size corrections are applied as a postprocessing tool following the methodology of Falletta *et. al.* [29] (see the Supplemental Material (SM), Sec. 1 [30]) to adjust all formation and trapping energies calculated herein. These finite-size corrections are of vital importance for the self-consistent calculation of the Hubbard-U parameter (see Sec. 2 of the SM [30]) according to Falletta *et al.* [16,29,31], which we apply to the 3*d* orbitals of Ti. We calculate the U parameter to be 4.26 eV (see Sec. 2 of the SM [30]).

To calculate the defect formation energy for the PVCs, the general defect formation energy for a defect with charge state, q, relaxed to a geometry, $R_{q'}$, may be written [29]

$$E_f(q, R_{q'}) = E_{\text{tot}}(q, R_{q'}) - E_{\text{tot}}(0, R_0) + q(\epsilon_v + \epsilon_F) - \sum_i n_i \mu_i + E_{\text{cor}}(q, R_{q'}). \quad (2)$$

The $E_{\text{tot}}(q, R_{q'})$ and $E_{\text{tot}}(0, R_0)$ terms represent the total energy of the defect and perfect systems, ϵ_v is the valence-band maximum (VBM) of the perfect system $(0, R_0)$, ϵ_F is the Fermi level within the band gap, n_i is the number of species i with chemical potential μ_i involved in defects in the system, and $E_{\text{cor}}(q, R_{q'})$ is the finite-size correction term for the defect, calculated via equation (S1). The relevant values for PTO are the oxygen chemical potential, $\mu_O = -4.388\,eV$, and the VBM of the perfect system, $\epsilon_v = 6.040\,eV$. For example, the notation for an electron polaron in PTO would be represented as $(-1, R_{-1})$, since the polaron is a charged defect, $q = -1$ (extra electron), with a geometry relaxed in response to charge state q, R_{-1}. For an oxygen vacancy, $q = +2$ (two electrons missing, $V_O^{\bullet\bullet}$), as the vacancy represents the removal of an oxygen ion, with a geometry also relaxed in the presence of a $+2$ charge, R_{2+}, resulting in $(+2, R_{+2})$.

Trapping energies, strain energies, and electronic energies are calculated according to the set of systems in Fig. 1(b) and Eq. (1) with an added correction for finite-size effects (see Sec. 1 of the SM [30]):

$$E_{\text{trap}} = E_{\text{loc}}^{\text{rel}} - E_{\text{del}}^{\text{unrel}} + E_{\text{cor}}. \quad (3)$$

Additionally, the binding energy between the polaron and the vacancy in the complexes may be calculated using formation energies calculated via Eq. (2):

$$E_{\text{bind}} = E_f(+1, R_{+1}) - E_f(-1, R_{-1}) - E_f(+2, R_{+2}), \quad (4)$$

where the $(+1, R_{+1})$ state represents the formation energy of the PVC, the $(-1, R_{-1})$ represents the formation of the bulk polaron, and the $(+2, R_{+2})$ is the formation energy of the bulk $+2$-charged oxygen vacancy. We therefore use Eq. (4) to quantify the energy associated with polaron and vacancy attraction to one another to form a complex.

All polarons, including those in the complexes, are calculated via the Deskins group [13,32,33] method (see Sec. 3 of the SM [30]), where a relaxed system with a single substitution at the site of interest is used to generate localized wave functions. These wave functions are used as a starting point for subsequent calculations, a kind of "reference state" from which a polaron may be localized. We study several complexes obtained by varying this reference state in three ways: (i) beginning from a vacancy with random wave functions and using the Deskins group method, (ii) starting from $+2$ charged vacancy wave functions and adding an electron,

TABLE I. The defect formation energy, E_f, for each defect as calculated by DFT + U ($^{+U}$) and standard DFT (^{PBE}), as well as the trapping energy, E_{trap} (for polarons), are compared to one another and to reference (^{REF}) energies. The defect formation energies were all calculated using Eq. (2) and the trapping energies by Eq. (3). The reference system used for the $(-1, R_{-1})$ polaron, Ti'_{Ti}, is the $(-1, R_0)$ system, while the semilocalized $V_O^{\bullet}$ system, $(1, R_1)$, is used as the reference for both PVCs. Note all formation energies are calculated with $\epsilon_F = 0$ eV.

Name	Defect	E_f^{+U} (eV)	E_f^{PBE} (eV)	E_{trap} (eV)	E_{strain} (eV)	E_{elect} (eV)	E_{bind} (eV)	E_f^{REF} (eV)	E_{trap}^{REF} (eV)
Bulk Polaron	Ti'_{Ti} (t2g)	1.882		−0.131	0.200	−0.331			−0.16 [12]
Neut. Vacancy	V_O^X	5.698	5.420					4.78 [23], 5.45 [32]	
Chg. Vacancy	$V_O^{\bullet\bullet}$	2.647	2.570					2.55 [23]	
eg Complex	$V_O^{\bullet\bullet} + Ti'_{Ti}$ (eg)	4.162		−0.138	0.028	−0.166	−0.367		
Semilocalized	$V_O^{\bullet}$	4.300	3.897				−0.228		
t2g Complex	$V_O^{\bullet\bullet} + Ti'_{Ti}$ (t2g)	4.393		0.092	0.381	−0.289	−0.136		

and (iii) previously localized polaron wave functions and subsequently adding a vacancy. Each of these reference states resulted in a distinct system with different energetics, lattice distortion, and electronic structure.

All charge and spin density analyses are performed using VESTA [34] for each polaron and/or vacancy system. Finally, the electronic structure is investigated for each system by calculating the orbital-resolved density of states (DOS) for both the up and down spin channels. These orbital and spin-resolved DOSs are compared to investigate the key differences among the PVCs, using our own Python code. Again, all energy values calculated in this work are subject to the corrections given in Eq. (2), utilizing the code provided by Falletta *et al.* [29].

III. RESULTS/DISCUSSION

A. Complex and individual defect formation energies

Taken together, the trapping energy, defect formation energy, and binding energy suggest that the *eg* complex is the preferred configuration for a +1-charged vacancy. First, trapping energies calculated using Eq. (3) reveal that the *eg* polaron is stable ($E_{trap} = -0.138$ eV) relative to the semilocalized solution ($V_O^{\bullet}$) near a vacancy; comparatively, the *t2g* polaron is unstable ($E_{trap} = 0.092$ eV) near a vacancy (see discussion in Sec. III B). This stability difference is primarily due to the very low cost of distorting the lattice in the *eg* complex ($E_{strain} = 0.028$ eV) and a much higher energy cost in the *t2g* complex ($E_{strain} = 0.381$ eV). The electronic transition energies for the *eg* (−0.166 eV) and *t2g* (−0.289 eV) complexes are much closer. The bulk polaron also has a less favorable trapping energy (−0.131 eV) than the *eg* complex, showing that the polaron is more easily trapped near a vacancy than in the bulk of PTO. The trapping energy of the bulk polaron calculated here agrees with hybrid functional trapping energy calculations of Ghorbani *et al.* [12] (Table I) (see the discussion in Sec. III C). Additionally, the complex and individual defect formation energies, calculated using Eq. (2), reveal a stability difference between the PVCs. The *eg* complex is the most energetically favorable configuration for an electron near an oxygen vacancy, with a formation energy of 4.162 eV, followed by the semilocalized electron near a vacancy at 4.300 eV, and the least energetically favorable is the *t2g* complex with a 4.393 eV formation energy (Table I). The binding energies, calculated via Eq. (4), show that the polaron and vacancy are most attracted to one another in the *eg* complex (−0.367 eV), and least attracted to one another in the *t2g* complex (−0.136 eV). Furthermore, the negative values for all the binding energies indicate that the electrons in any form studied here are attracted to the oxygen vacancy. The oxygen vacancy formation energies calculated agree with those calculated by Zhang *et al.* [23] and Tomoda *et al.* [35] using DFT + U and hybrid calculations, respectively (see Sec. 4 of the SM [30] and Ref. [36] therein for additional comparison involving structure, dielectric properties, and defect formation energies).

B. Oxygen vacancy-polaron complexes

The ionic displacements, spin density, and charge density of different complex configurations shown in Fig. 4 reveal marked differences between the complexes. In the *eg* complex [Fig. 2(a)], the spin density resembles a distended bottle-shape in a Ti-3d_{eg} (*eg* from here on) state originating from the 1NN Ti-site to the oxygen vacancy. This 1NN Ti-site is also the site with the greatest ionic displacement, relative to the $V_O^{\bullet\bullet}$ system, while oxygen ions (negative) displace away, and lead ions (positive) displace toward the vacancy. The charge density [Fig. 2(e)] reflects the spin density, also occurring primarily on the 1NN Ti-site, again in a distended bottle shape that extends into the oxygen vacancy site. This spin density matches that found by Xu *et al.* [22] using hybrid functionals, where electrons trapped at vacancies become magnetic as they are in this work. On the other hand, the *t2g* complex spin density [Fig. 2(b)] has the clover-shape of the Ti-3d_{t2g} (*t2g* from here on) orbital, accompanied by ionic displacements primarily occurring in response to the polaron itself. That is, the ionic displacement pattern shows no displacement of the 1NN Ti-site hosting the polaron, and displacement of the 1NN ions occurs toward or away from the polaron rather than the vacancy. The charge density difference [Fig. 2(f)] also shows a reduction in the charge density along the Ti-O bonding directions and an increase in the charge density at the 1NN Ti-site in the shape of the *t2g* orbital, whose lobes extend between the in-plane oxygen ions. These subtle differences lead to instability in the *t2g* complex, resulting in a preference for the polaron to localize in the *eg* orbital of the 1NN Ti-ion.

Interestingly, the semilocalized system resembles the *eg* complex in both charge density changes [Figs. 2(e) and 2(g)] and the ionic displacements; however, they differ significantly in their spin densities [Figs. 2(a) and 2(c)]. In the *eg* complex,

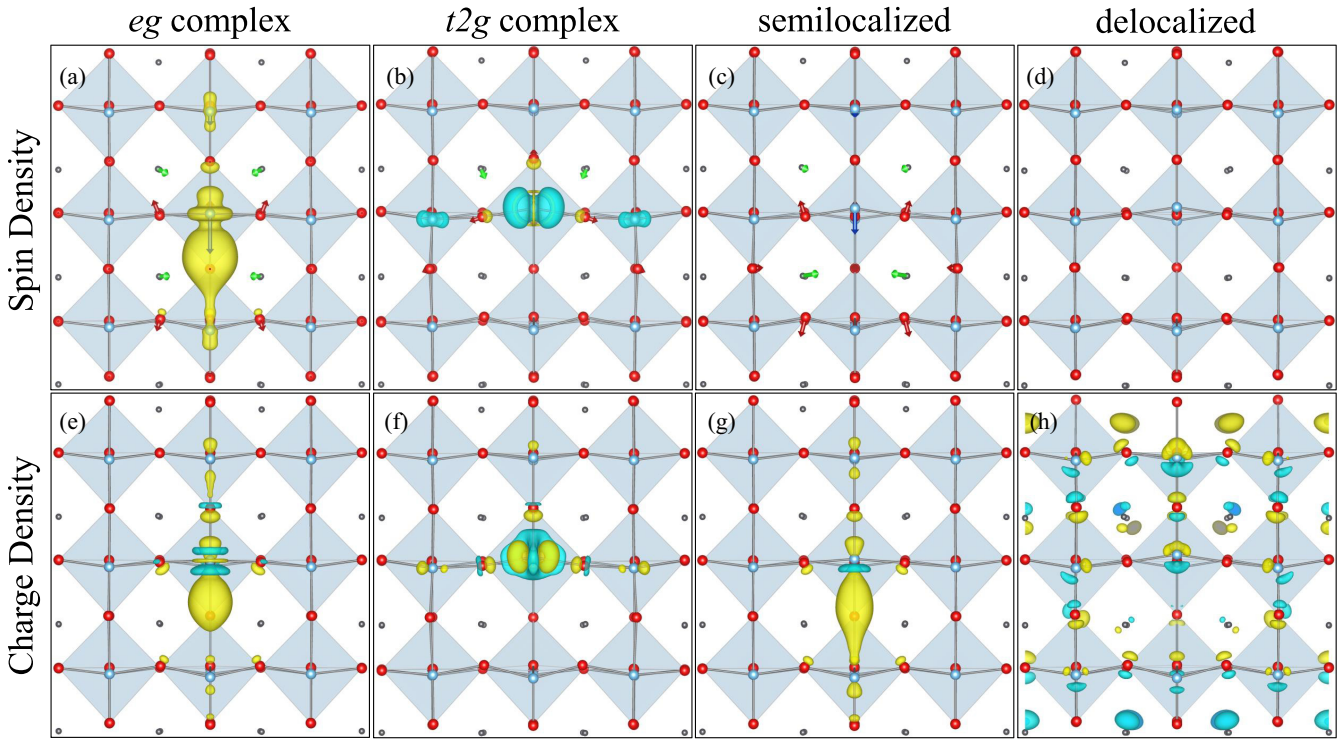

FIG. 2. The spin density and ionic displacements are shown in the top row for the $V_O^{\bullet\bullet} + Ti_{Ti}'^{(eg)}$ system (*eg* complex), the $V_O^{\bullet\bullet} + Ti_{Ti}'^{(t2g)}$ system ($t2g$ complex), the $V_O^{\bullet}$ DFT + U system (semilocalized), and the $V_O^{\bullet}$ standard DFT system (delocalized). The charge density differences are taken between the +1 electron and +0 electron systems in the same lattice configuration to show where the added electron charge density localizes. Isosurface levels are at 0.0035 $e^-/Å^3$ for both spin and charge densities, and displacement vectors are scaled up by 5× for ease of viewing. The dark gray atoms (green arrows) are Pb, the silver atoms (blue arrows) are Ti, and the red atoms (red arrows) are O. Note that the supercell has been sliced to remove the part obstructing the view of the complex, and for ease of comparison with other structures in this work.

the spin density reveals a single electron localized to the 1NN *eg* orbital, while there is no localized spin density in the semilocalized system, suggesting at most only partially occupied states with paired electrons. Other minor differences occur in the ionic displacements via the relative magnitudes of given sites, where the 1NN Ti-site displaces more (∼0.1 Å) and the 1NN O-sites and 1NN Pb-sites displace slightly less in the *eg* complex. Additionally, the difference in the charge density map reveals that the extra electron localizes more completely on the 1NN Ti-site in the *eg* complex [Figs. 2(e) and 2(g)]. That is, the semilocalized system has a charge density change extending between two Ti-sites across the vacancy, whereas the *eg* complex has a more localized change.

In the delocalized system, calculated by standard DFT [Figs. 2(d) and 2(h)], there is no spin density change, and the charge density for the single added electron is spread throughout the supercell. This is due to the lack of charge localization in standard DFT. Furthermore, the single delocalized electron does not significantly impact the ionic positions, resulting in displacements <0.01 Å. Indeed, the treatment of extra electrons in standard DFT results in too little change to the system when compared with any of the other systems, instead giving a result suggesting the electrons and vacancy interact only a little.

The orbital-resolved DOS shows that both the *eg* and $t2g$ complexes have a midgap state at 1.35 eV, while both the semilocalized and delocalized systems possess no midgap state (Fig. 3). These midgap states show the polaronic nature of the defect, composed of unpaired electrons (see the insets of Fig. 3) of primarily one orbital character, *eg* in the *eg* complex and $t2g$ in the $t2g$ complex. On the other hand, there is no difference between the spin-up and spin-down DOS of the semilocalized and delocalized systems, showing that these oxygen vacancy systems do not have polarons present as all electrons are paired. Instead, states appear in the semilocalized system at the CBM, and little change occurs in the electronic structure of the delocalized system.

A comparison of the orbital character of the midgap states in the *eg* and $t2g$ complexes indicates that the primary electronic difference between them is the orbital that the polaron occupies, showing PVIs can cause a shift in the energy of the orbitals at the nearest-neighbor ion site hosting the polaron. That is, the *eg* orbitals composing the midgap state in the *eg* complex may be found in the conduction band of the $t2g$ complex DOS (see the black arrows in Fig. 3), and vice versa. In the $t2g$ complex, this produces an energetically unfavorable result (Table I), meaning that a shift of the *eg* orbitals to lower energy than the $t2g$ orbitals on the polaron site is the correct physical picture of the system. This suggests how the orbital degree of freedom may be affected by defects.

Despite the similarity between the charge densities of the semilocalized system and the *eg* complex, the spin-resolved DOS (insets in Fig. 3) shows that the two are electronically quite different. The semilocalized case lacks a midgap state; instead, all the electrons are paired, and the states added at the CBM partially occupy both the up and down spin channels.

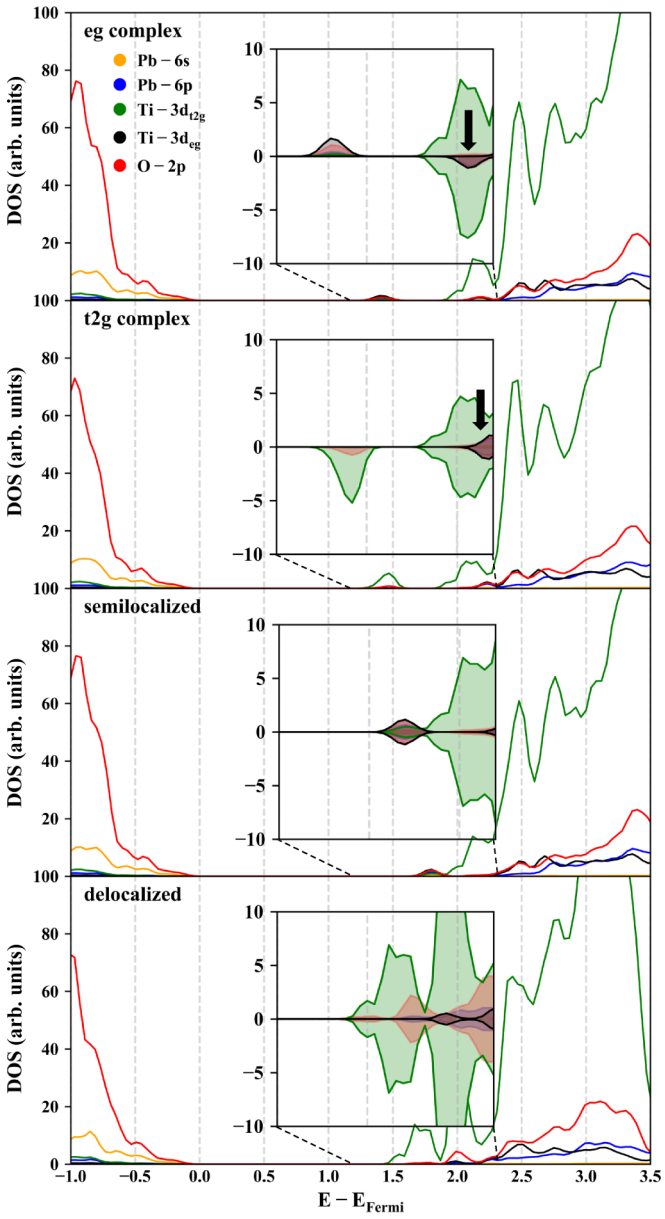

FIG. 3. The pDOSs of the *eg* complex, the *t*2*g* complex, the semilocalized system, and the delocalized system are shown. Each inset figure is from 1.0 to 2.2 eV, and the data therein are separated by a spin channel into positive (spin-up) and negative (spin-down). All pDOSs are in arbitrary units, and arrows are added for ease of discussion.

Furthermore, this state is found to originate from several orbitals across both Ti and O species, consistent with a lack of spin density (i.e., all electrons are paired) and a charge density spread between several sites. Therefore, the charge density change for the semilocalized system is not representative of a polaron like those of either complex. Still, the semilocalized state is found to be more energetically favorable than the *t*2*g* complex (Table I), even though a polaron is found to be more energetically favorable than a delocalized electron in the bulk. A vacancy, therefore, appears to interfere with the stability of the *t*2*g* polaron and increase the stability of the *eg* complex by lowering the energy cost of distorting the lattice into the *eg* complex configuration, which increases the cost of distorting the lattice into the *t*2*g* complex configuration.

The standard DFT level of theory is shown to have a drastically different description of the electronic structure of the $V_O^{\bullet}$ system, resulting in an unphysical picture of the charge-vacancy interaction (Fig. 3). The delocalized system is hallmarked by both the lack of a midgap state and delocalization of the charge across the supercell used in the calculation (Fig. 2), which is reflected in the orbital-resolved DOS by the delocalization of the added electron across many sites, and both spin-channels. Therefore, we find that the standard level of DFT, even with finite-size corrections as in this work, is not adequate for describing the lowest energy state of the $V_O^{\bullet}$ system.

C. Bulk polaron, $Ti'^{(t2g)}_{Ti}$

To compare with the complexes and previous literature, we carried out bulk polaron calculations. In Fig. 4(a), the spin density matches the 3D cloverlike structure of a *t*2*g* orbital in the plane of the Ti-ion layer. The ionic displacements near the polaron show the nominally Pb^{2+} ions moving toward it by 0.027 Å, while the O ions move away by ∼0.06 Å, and no displacement occurs at all on the host Ti-site. This results in Ti-O bond lengthening of 0.061 Å in the *x*-*y* plane and 0.065 Å in the *z* plane. The spin and charge density shows the bulk polaron contains the same orbital structure as the *t*2*g* complex, where charge density is lost along the bonding directions near the polaron site and gained in the cloverlike pattern found in the spin density figure [Fig. 4(a)]. This is consistent with the bond lengthening found in the ionic displacements. Analysis of the electronic structure of the bulk polaron [Fig. 4(b)] reveals the addition of a midgap state at 1.3 eV, relative to the pristine system. The midgap state is primarily of *t*2*g* character, and the states are contributed by a single Ti-site. As expected, the delocalized system lacks this state, and instead only shows small changes made at the CBM, relative to the pristine system. Overall, we find the character of the bulk self-trapped electron polaron in PTO to be a localized *t*2*g* state with 1NN oxygen ions displacing away from the polaron. These calculations show good agreement with hybrid functional calculations of Ghorbani *et al.* [12] concerning the structure, polaron shape, and polaron trapping energy (see Sec. 4.0 of the SM).

Comparing the bulk polaron with the *t*2*g* complex reveals that the ionic displacements, spin density, and charge densities are virtually identical [Figs. 2 and 4(a)]. The ionic displacements have the same pattern in both systems, where the 1NN O-sites displace outward from the polaron Ti-site, while the polaron site itself displaces only negligibly. The charge and spin densities reveal the same clover pattern of a *t*2*g* orbital in both systems as well. It appears the *t*2*g* complex is essentially the bulk polaron configuration placed at the 1NN Ti-site of the vacancy. This, however, becomes energetically unstable near the vacancy and prefers to reorient into the *eg* complex configuration (Table I). Furthermore, the *t*2*g* complex (Fig. 3) and bulk polaron [Fig. 4(b)] midgap states have a nearly identical structure at the same energy relative to the VBM (localization into the up or down spin channels is equivalent herein). However, a key difference is the *eg* orbital states found

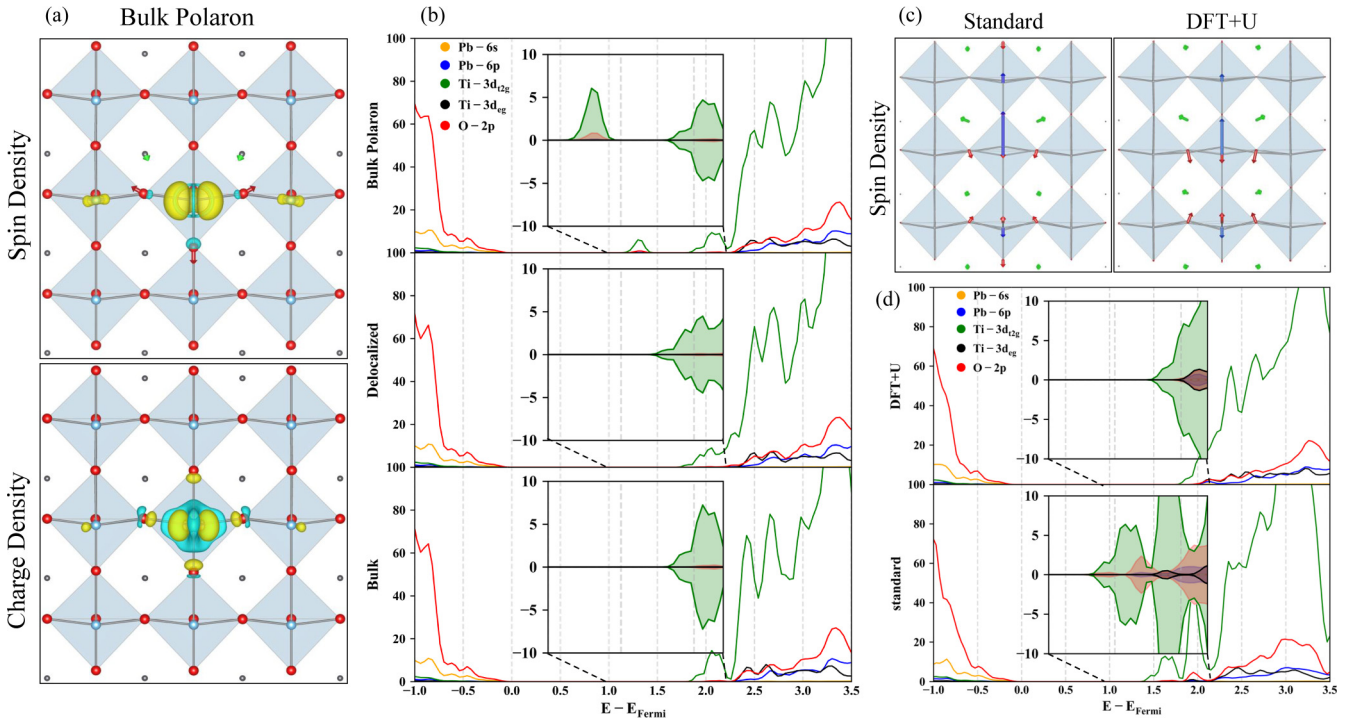

FIG. 4. (a) The spin density and ionic displacements of the bulk polaron are shown on the top, while the charge density difference generated by the polaron is shown on the bottom. (b) The orbital-resolved DOS for the bulk polaron, the delocalized system, and the bulk system are compared with an inset displaying spin-polarized data for a region of the band gap and CBM. (c) The spin density and ionic displacements of a +2 charged oxygen vacancy are shown on the left for standard DFT (Standard) and on the right for DFT + U (DFT + U). (d) The orbital-resolved DOS of the +2 charged vacancy species is shown for the DFT + U (upper) and standard DFT (lower) levels of theory. All pDOS are in arbitrary units, and all spin/charge density figures are constructed the same as in Fig. 2.

just within the conduction bands of the $t2g$ complex (see the black arrows in Fig. 3), which are from the 1NN Ti-ion where the polaron is localized. That is, the *eg* orbitals composing the midgap state of the *eg* complex are not present near the CBM of the bulk polaron, but they are present in the $t2g$ complex. This is due to the removal of an oxygen ion, which would lower the energy of the 1NN Ti *eg* orbitals by providing additional space to accommodate a polaron.

D. Oxygen vacancies in the bulk

As a reference, we perform simulations of an oxygen vacancy in the bulk using standard DFT and DFT + U. The difference between the ionic structures and spin densities of the +2 charged vacancy species calculated by standard DFT and DFT + U is very small [Fig. 4(c)]. The spin densities in both cases are on the order of $<10^{-6}\,e^{-}/\text{Å}^3$, which is essentially negligible since all electrons are paired together. The ionic displacements near the vacancy are also nearly the same, the largest difference being the 1NN Ti-site moving slightly further in the standard DFT case, and 1NN O-sites moving slightly further in the DFT + U case. Essentially, the 1NN Ti- and Pb-sites move away from the vacancy, while the 1NN O-ions move toward it. Furthermore, the charge density figures for both the standard and DFT + U cases reveal that the charge density change is delocalized across the ionic sites surrounding the vacancy itself, rather than appearing to be confined to a particular orbital. In fact, it is known that the standard DFT obtains delocalized solutions for systems it considers, and is not suitable for calculating polarons as a result [1].

Despite the similarity in the formation energy and ionic structures, there are significant differences between the electronic structures for the DFT + U and standard DFT cases. In the DFT + U case, the conduction-band edge is pushed to higher energies and is composed mostly of $t2g$ states, increasing the band gap by nearly 1 eV compared to the standard DFT case. This still gives a band gap of 1.6 eV, which has better agreement with the experimental value of 3.6 eV [11], but still significantly underestimates it. However, the underestimation of the band gap using a U parameter is expected and does not impact the validity of the results calculated for the polarons (see Sec. 6 of the SM [30] for discussion on the band gap and charge transfer levels). In the standard DFT case, the states composing conduction bands spread out to lower energies, and mixing between Ti-3*d* and O-2*p* increases, resulting in a smaller band gap. This difference in the electronic structure shows the importance of the DFT + U formalism for calculating the electronic structure of defects. However, simply using the DFT + U formalism is not enough when subtler effects on the electronic structure must be considered, as shown in the sections on the polaron-vacancy complex and bulk polaron (Secs. III B and III C, respectively).

IV. CONCLUSIONS AND DISCUSSIONS

These results contribute to our overall understanding of PVIs in several ways. First, PVCs can be treated with

DFT + U to achieve greater computational efficiency and maintain accuracy compared to hybrid functionals, but they must be treated with subtlety. We find several local minima by varying the initial conditions in three ways: (i) Beginning from an oxygen vacancy system with random wave functions and subsequently localizing a polaron, (ii) beginning from an oxygen vacancy system with oxygen vacancy wave functions and attempting to localize a polaron, and (iii) starting from the bulk polaron system and wave functions and subsequently introducing an oxygen vacancy. We find that method (i) results in the correct physical picture in PTO, giving the most energetically favorable complex with a polaron in a first-nearest-neighbor *eg* orbital. Method (ii) results in a "semilocalized" system with the added electron shared among several ions near the oxygen vacancy, but not resulting in a polaron. Method (iii) gives an unstable PVC, with a polaron in a $t2g$ orbital. We find simulating the polaron-defect complex by first introducing the defect and allowing the polaron to be localized starting from random wave functions is the best method.

Second, the *eg* complex is found to be the most energetically stable because the vacancy acts to significantly decrease (increase) the strain energy cost of a polaron trapped in the *eg* ($t2g$) orbital of the nearest-neighbor Ti-ion (Table I). This is reflected by the spin/charge density (Fig. 2), which occupies the space left behind in the oxygen vacancy in the *eg* complex but occupies the space above the vacancy in the $t2g$ complex. Furthermore, the displacements caused by the polaron in the *eg* complex cause octahedral tilting instead of displacement directly into the oxygen octahedra as in the $t2g$ complex (Fig. 2). This strain-lowering effect of the vacancy outcompetes the smaller electronic transition energy associated with occupying the *eg* orbital instead of the $t2g$ orbital (Table I). Indeed, the electronic structure of the *eg* complex shows the energy of *eg* orbitals on the 1NN Ti-ion lowering into the band gap, while the energy of the $t2g$ states remains in the conduction bands (Fig. 3). These results show that the *eg* complex is the correct physical picture of the polaron-vacancy complex, where the polaron occupies a Ti-ion *eg* orbital in the space provided by the oxygen vacancy.

Third, electrons and polarons in PTO are generally attracted to oxygen vacancies as all calculated binding energies are negative (E_{bind}, Table I). Then, comparing the bulk polaron and *eg* complex trapping energies shows that the bulk polaron could lower its energy by binding with a vacancy to form an *eg* complex. Overall, this paints a physical picture where electrons, either itinerant or trapped, in the bulk of PTO are attracted to oxygen vacancies that significantly lower the strain energy of occupying the 1NN Ti-ion *eg* orbitals. Additionally, these results appear to be general, applying not only to other perovskites, but also to other transition-metal oxides. For example, Janotti *et al.* [5] use hybrid functionals to calculate polaron-oxygen vacancy complexes in $SrTiO_3$ (STO), resulting in several configurations, and polarons have been invoked to explain the resistive switching behavior in CeO_2 [4,14]. Finally, experimental results from Crespillo *et al.* [37–39] showed that a luminescence peak that increased with increasing oxygen vacancy concentration was due to a shift from conduction electrons in $t2g$ orbitals to a midgap state composed of *eg* orbitals at the oxygen vacancy, similar to what is predicted here for PTO.

This work lays the foundation for additional exploration of polaron engineering in PTO and in other oxides by utilizing strain and defects to affect polaron properties. For instance, understanding the influence of epitaxial strain on polarons and PVCs may lead to more precise control over polaron stability and optical transitions.

The data used to generate the figures given in this article are available upon reasonable request.

ACKNOWLEDGMENTS

This research was primarily supported by the National Science Foundation Materials Research Science and Engineering Center program through the UT Knoxville Center for Advanced Materials and Manufacturing (DMR-2309083). This project used computational resources via the Infrastructure for Scientific Applications and Advanced Computing (ISAAC) Secure Enclave and ISAAC Next Gen at the University of Tennessee-Knoxville.

[1] C. Franchini, Polarons in materials, Nat. Rev. Mater. **6**, 560 (2021).

[2] M. Reticcioli, Interplay between Adsorbates and Polarons: CO on Rutile TiO_2(110), Phys. Rev. Lett. **122**, 016805 (2019).

[3] D. Zhang, Oxygen-vacancy dynamics and entanglement with polaron hopping at the reduced CeO_2(111) surface, Phys. Rev. Lett. **122**, 096101 (2019).

[4] L. Sun, Polaronic resistive switching in ceria-based memory devices, Adv. Electron. Mater. **5**, 1900271 (2019).

[5] A. Janotti, Vacancies and small polarons in $SrTiO_3$, Phys. Rev. B **90**, 085202 (2014).

[6] E. Pastor, Electronic defects in metal oxide photocatalysts, Nat. Rev. Mater. **7**, 503 (2022).

[7] C. Freysoldt, First-principles calculations for point defects in solids, Rev. Mod. Phys. **86**, 253 (2014).

[8] S. L. Dudarev, Electron-energy-loss spectra and the structural stability of nickel oxide: An LSDA+U study, Phys. Rev. B **57**, 1505 (1998).

[9] A. Filippetti and N. A. Spaldin, Self-interaction-corrected pseudopotential scheme for magnetic and strongly-correlated systems, Phys. Rev. B **67**, 125109 (2003).

[10] J. P. Perdew and A. Zunger, Self-interaction correction to density-functional approximations for many-electron systems, Phys. Rev. B **23**, 5048 (1981).

[11] D. I. Bilc, Hybrid exchange-correlation functional for accurate prediction of the electronic and structural properties of ferroelectric oxides, Phys. Rev. B **77**, 165107 (2008).

[12] E. Ghorbani, Self-consistent calculations of charge self-trapping energies: A comparative study of polaron formation and migration in $PbTiO_3$, Phys. Rev. Mater. **6**, 074410 (2022).

[13] M. Setvin, Direct view at excess electrons in TiO_2 rutile and anatase, Phys. Rev. Lett. **113**, 086402 (2014).

[14] L. Sun, Disentangling the role of small polarons and oxygen vacancies in CeO_2, Phys. Rev. B **95**, 245101 (2017).

[15] P. Erhart, Efficacy of the DFT + U formalism for modeling hole polarons in perovskite oxides, Phys. Rev. B **90**, 035204 (2014).

[16] S. Falletta and A. Pasquarello, Hubbard U through polaronic defect states, npj Comput. Mater. **8**, 263 (2022).

[17] M. Cococcioni and S. De Gironcoli, Linear response approach to the calculation of the effective interaction parameters in the LDA+U, Phys. Rev. B **71**, 035105 (2005).

[18] J. F. Janak, Proof that $\frac{\partial E}{\partial n_i} = \varepsilon$ in density-functional theory, Phys. Rev. B **18**, 7165 (1978).

[19] A. Janotti, Hybrid functional studies of the oxygen vacancy in TiO_2, Phys. Rev. B **81**, 085212 (2010).

[20] R. I. Eglitis, E. A. Kotomin, and G. Borstel, Quantum chemical modelling of "green" luminescence in ABO_3 perovskites, Eur. Phys. J. B **27**, 483 (2002).

[21] T. Shimada, Y. Uratani, and T. Kitamura, Vacancy-driven ferromagnetism in ferroelectric $PbTiO_3$, Appl. Phys. Lett. **100**, 162901 (2012).

[22] T. Xu, Multiferroic domain walls in ferroelectric $PbTiO_3$ with oxygen deficiency, Nano Lett. **16**, 454 (2016).

[23] L. Zhang, Oxygen vacancy formation energies in $PbTiO_3/SrTiO_3$ superlattice, Phys. Rev. Mater. **2**, 064409 (2018).

[24] G. Kresse and J. Furthmüller, Efficiency of *ab-initio* total energy calculations for metals and semiconductors using a plane-wave basis set, Comput. Mater. Sci. **6**, 15 (1996).

[25] G. Kresse and J. Furthmüller, Efficient iterative schemes for *ab initio* total-energy calculations using a plane-wave basis set, Phys. Rev. B **54**, 11169 (1996).

[26] J. P. Perdew, Restoring the density-gradient expansion for exchange in solids and surfaces, Phys. Rev. Lett. **100**, 136406 (2008).

[27] L. Zhang, Oxygen vacancy diffusion in bulk $SrTiO_3$ from density functional theory calculations, Comput. Mater. Sci. **118**, 309 (2016).

[28] P. E. Blöchl, Projector augmented-wave method, Phys. Rev. B **50**, 17953 (1994).

[29] S. Falletta, J. Wiktor, and A. Pasquarello, Finite-size corrections of defect energy levels involving ionic polarization, Phys. Rev. B **102**, 041115 (2020).

[30] See Supplemental Material at http://link.aps.org/supplemental/10.1103/PhysRevMaterials.8.094406 for further information on the application of finite-size corrections (Sec. 1) in this work, and their use in enforcing piecewise-linearity and the self-consistent calculation of the Hubbard-U parameter applied to Ti (Sec. 2). The methodology for calculating polarons as part of vacancy complexes and in the bulk is discussed in greater detail in Sec. 3. Additionally, comparison with previous literature on $PbTiO_3$ is made concerning our calculated structrure, dielectric properties, and defect formation energies (Sec. 4). Finally, calculated charge transfer levels including bulk polarons and polaron-vacancy complexes as compared to oxgyen vacancies within the band gap are discussed (Sec. 5).

[31] S. Falletta and A. Pasquarello, Polarons free from many-body self-interaction in density functional theory, Phys. Rev. B **106**, 125119 (2022).

[32] N. A. Deskins and M. Dupuis, Electron transport via polaron hopping in bulk TiO_2: A density functional theory characterization, Phys. Rev. B **75**, 195212 (2007).

[33] T. D. Pham and N. A. Deskins, Efficient method for modeling polarons using electronic structure methods, J. Chem. Theory Comput. **16**, 5264 (2020).

[34] K. Momma and F. Izumi, VESTA 3 for three-dimensional visualization of crystal, volumetric and morphology data, J. Appl. Crystallogr. **44**, 1272 (2011).

[35] S. Tomoda, Hybrid functional study on the ferroelectricity of domain walls with O-vacancies in $PbTiO_3$, Mech. Eng. J. **2**, 15-00037 (2015).

[36] A. G. Kalinichev, Elastic properties of tetragonal $PbTiO_3$ single crystals by Brillouin scattering, J. Mater. Res. **12**, 2623 (1997).

[37] M. Crespillo, Recent advances on carrier and exciton self-trapping in strontium Titanate: Understanding the luminescence emissions, Cryst. **9**, 95 (2019).

[38] M. L. Crespillo, Role of oxygen vacancies on light emission mechanisms in $SrTiO_3$ induced by high-energy particles, J. Phys. D **50**, 155303 (2017).

[39] M. L. Crespillo, Isolated oxygen vacancies in strontium titanate shine red: Optical identification of Ti^{3+} polarons, Appl. Mater. Today **12**, 131 (2018).